Turkish Journal of Electrical Engineering & Computer Sciences

http://journals.tubitak.gov.tr/elektrik/

Research Article

Turk J Elec Eng & Comp Sci
(2014) 22: 1116 – 1129

doi:10.3906/elk-1210-60

Application of Hilbert–Huang transform and support vector machine for detection and classification of voltage sag sources

Alireza FOROUGHI[1], **Ebrahim MOHAMMADI**[1], **Saeid ESMAEILI**[2,*]
[1]Department of Electrical and Computer Engineering, Graduate University of Advanced Technology, Kerman, Iran
[2]Department of Electrical Engineering, Shahid Bahonar University of Kerman, Kerman, Iran

Received: 14.10.2012 • **Accepted:** 04.02.2013 • **Published Online:** 15.08.2014 • **Printed:** 12.09.2014

Abstract: Power quality disturbances, including voltage sag, swell, harmonics, flicker, and notch, are one of the main concerns for industries and electrical equipment. Among these disturbances, voltage sag, due to its irrecoverable economic effects on industries, is particularly important. In this paper, the detection and classification of voltage sag sources containing motor starting, short circuit, transformer energizing, and the reacceleration of motors after fault clearance using the Hilbert–Huang transform (HHT) and support vector machine (SVM) are studied. A voltage sag waveform includes several oscillating modes; for separating these oscillating modes, which are called intrinsic mode functions (IMFs), empirical mode decomposition is used. Next, by applying the HHT to these IMFs, some required features of each IMF are extracted. Finally, these features are given to the SVM for classification. The results of this classification method as compared with other methods show the high efficiency of the proposed method.

Key words: Voltage sag classification, Hilbert–Huang transform, support vector machine, empirical mode decomposition, intrinsic mode function, power quality

1. Introduction

In recent years, because of an incremental use of voltage-sensitive equipment and power electronic devices, power quality has become more remarkable. The first step for improving power quality is the detection of power quality disturbances. For this purpose, a method is needed to extract and analyze the waveform information and detect the type and cause of the disturbance. One of the most important power quality disturbances is voltage sag, which is defined as a reduction of the root mean square (RMS) voltage of between 0.1 (p.u.) and 0.9 (p.u.) at the power frequency for a duration of half a cycle to 1 min [1]. The main causes of voltage sag are short circuits, motor starting, transformer energizing, and the reacceleration of motors after a fault clearance.

The detection and classification of power quality disturbances have been studied in several papers. In [2], power quality disturbances were classified using the wavelet transform and support vector machine (SVM). The classification of power quality disturbances by applying the Stockwell transform (S-transform) and neural networks was studied in [3]. Moreover, the advantages of the S-transform compared with the wavelet transform were presented. Application of the Hilbert transform and neural networks for the detection of power quality disturbances was described in [4]. In [5], the theoretical and practical aspects of different methods for the definition, characterization, and classification of voltage sag and interruptions and their shortfalls were studied.

*Correspondence: s_esmaeili@uk.ac.ir

Voltage sag classification using the Hilbert transform and neural networks was considered in [6]. In [7], voltage sag causes were classified based on the generalized S-transform.

In [8], a method for the detection and classification of voltage sag disturbances based on the RMS voltage was proposed. In this method, some characteristics of a voltage sag waveform, such as the amplitude of the voltage sag, happening of the voltage jump at the end of the sag, balance of 3 phase voltages, and voltage swell happening, are extracted from the RMS voltage. Next, based on these features, the voltage sags are classified.

A simple rule-based method for the detection and classification of the voltage sag, swell, and interruption by applying the filter bank and adaptive filter was used in [9]. In this study, the actual recorded waveforms were used. The classification of voltage sag causes using the wavelet transform and probabilistic neural network was studied in [10]. In [11], voltage sags due to different types of short-circuit faults, including a 3-phase fault, phase-to-phase fault, double-phase-to-ground fault, and single-phase-to-ground fault, were classified by considering the transformer winding connection.

In this paper, the detection and classification of voltage sag sources based on the Hilbert-Huang transform (HHT) and SVM is considered. In the first step, by applying empirical mode decomposition (EMD) to the voltage sag waveform, the first 3 intrinsic mode functions (IMFs) are extracted. EMD is a technique that is used for analyzing nonlinear and nonstationary signals [12]. IMFs are monocomponent signals that are generated by the decomposition of a nonstationary signal. After extraction of the IMFs from the voltage sag waveform, the HHT is applied to the first 3 IMFs to extract 3 features, including the standard deviation of the magnitude, standard deviation of the phase, and energy distribution. Next, these features are given to the SVM for classification. Four voltage sag sources are considered, containing short circuits, motor starting, transformer energizing, and reacceleration of the induction motors after fault clearance. Moreover, the advantages and disadvantages of the S-transform, wavelet transform, and Hilbert transform are compared in this paper and, finally, the results of the classification using the HHT and SVM are compared with the wavelet transform and neural networks. The high efficiency of the proposed method shows the value of this method.

2. Empirical mode decomposition

A nonlinear waveform can include several frequency components. EMD is the extraction of monocomponent signals from a nonlinear and nonstationary signal. Every monocomponent signal that is extracted from a nonstationary signal is called an IMF. Extraction of IMFs is implemented based on the sifting process, in which the lowest frequency components are removed until the highest frequency component remains. A monocomponent signal is an IMF if it satisfies the following conditions:

a) The number of zero-crossing points and the number of extrema should be equal or differ only by 1.

b) The local average at any point obtained by the local maxima and the local minima is equal to 0.

The stages of extracting IMFs from the original signal are as follows [13]:

1. Identifying the upper envelope of signal by connecting the local maxima.

2. Similar to the first stage, identifying the lower envelope of the signal by connecting the local minima.

3. Obtaining the mean value of the upper and lower envelopes, which is defined as m (t).

4. The difference between the main signal x (t) and the mean value of the envelopes m (t) is the first component, which is represented in Eq. (1).

$$h_1(t) = x(t) - m(t) \tag{1}$$

5. If h_1 (t) satisfies the 2 above conditions, it is known as the first IMF of the main signal x (t); otherwise,

h_1 (t) is considered as the original signal and stages 1 to 4 are repeated until h_{11} (t), according to Eq. (2), is obtained:

$$h_{11}(t) = h_1(t) - m_1(t). \tag{2}$$

6. Stage 5 is repeated until h_{1k}, according to Eq. (3), as the first IMF is obtained.

$$h_{1k}(t) = h_{1(k-1)}(t) - m_{1k}(t) \tag{3}$$

7. $_r1$ (t) is a subtraction of the first IMF from the original signal, which is represented in Eq. (4).

$$r_1(t) = x(t) - h_{1k}(t) \tag{4}$$

8. $_r1$ (t) is considered as the original signal and steps 1 to 7 are repeated until the second IMF is obtained.

9. The above steps are repeated until n IMFs are obtained.

10. The decomposition procedure is stopped when $_rn$ (t) becomes a monocomponent signal and there are no more IMFs for extraction.

The algorithm for extracting the IMFs from the original signal is shown in Figure 1.

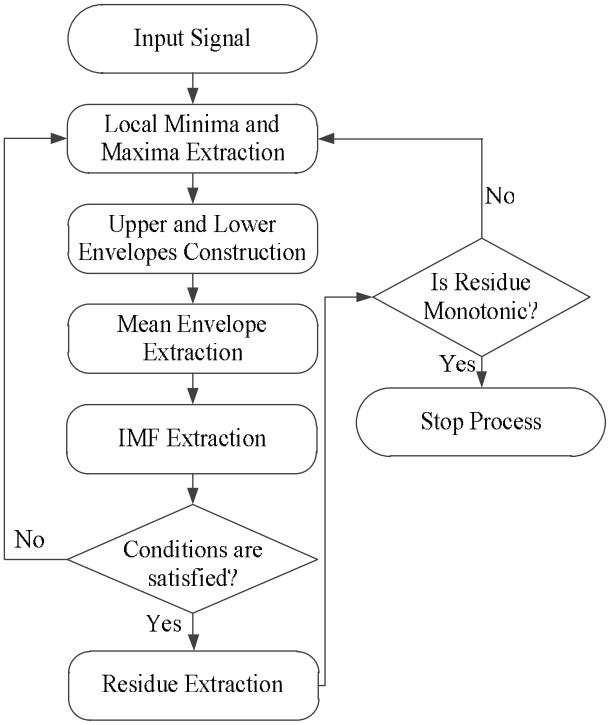

Figure 1. Flow chart of the EMD process.

3. The HHT

The HHT is a combination of the EMD method and the Hilbert transform [14]. After applying the EMD method and extracting the IMFs of a nonstationary signal, the Hilbert transform is used to obtain instantaneous frequency and instantaneous phase. The HHT is one of the best methods for analyzing nonlinear and nonstationary signals in a time-frequency domain. Table 1 illustrates the comparison among the HHT, wavelet transform, and Fourier transform [15,16]. It is obvious from Table 1 that the HHT is a powerful and reliable

method for analyzing nonlinear and nonstationary signals because it is based on an adaptive basis. Instantaneous frequency is obtained by differentiation instead of convolution. Thus, there is no limitation because of the uncertainty principle. This method is applicable for nonlinear and nonstationary signals. The outputs of this method are in the time-frequency-energy space and instantaneous phase, frequency, and energy distribution can be extracted as features of nonstationary signals.

Table 1. Comparison of the Fourier, wavelet, and Hilbert transform characteristics.

	Fourier	Wavelet	Hilbert
Basis	A priori	A priori	Adaptive
Frequency	Convolution: global uncertainty	Convolution: regional uncertainty	Differentiation: local, certainty
Presentation	Energy-frequency	Energy-time-frequency	Energy-time-frequency
Nonlinear	No	No	Yes
Nonstationary	No	Yes	Yes
Feature extraction	No	Discrete: no; continuous: yes	Yes
Theoretical base	Theory complete	Theory complete	Empirical

For obtaining an instantaneous phase, real and imaginary parts of the signal are required. The Hilbert transform converts a real-time domain signal, such as x (t), to another real-time domain signal, such as $\hat{x}(t)$ [17]. Thus, z (t), which is defined in Eq. (5), is used for analyzing:

$$z(t) = x(t) + j\hat{x}(t). \tag{5}$$

The Hilbert transform of a continuous signal x (t) is obtained from Eq. (6), as follows:

$$\hat{x}(t) = H\left[x(t)\right] = \int_{-x}^{x} \frac{x(u)}{\pi(t-u)} du, \tag{6}$$

where $\hat{x}(t)$ is the Hilbert transform of signal x (t), which is a convolution of signal x (t) and $\frac{1}{\pi t}$, as in Eq. (7):

$$\hat{x}(t) = x(t) * (\frac{1}{\pi t}). \tag{7}$$

The instantaneous phase and amplitude of signal x (t) can be obtained from Eq. (5), as follows:

$$A(t) = \left[x^2(t) + j\hat{x}^2(t)\right]^{\frac{1}{2}}, \tag{8}$$

$$\theta(t) = \tan^{-1}\left[\frac{\hat{x}(t)}{x(t)}\right], \tag{9}$$

$$f_0 = \frac{1}{2\pi t}\tan^{-1}\left[\frac{\hat{x}(t)}{x(t)}\right], \tag{10}$$

where $A(t)$ is the amplitude of the signal, $\theta(t)$ is the instantaneous phase, and f_0 is the instantaneous frequency.

4. Extraction of the required features by applying the Hilbert transform on the IMFs

After obtaining the IMFs of the signal using the EMD method, in the next step, the required features should be extracted from the IMFs. In this study, the features of the first 3 IMFs are extracted because the most frequency content of a signal is in these 3 IMFs and these features are sufficient for the detection and classification of voltage sag sources. These features include the energy distribution, standard deviation of the amplitude, and standard deviation of the phase. Therefore, there are 3 features for each IMF and a total of 9 features for the 3 IMFs of a voltage sag signal, which are used for classification.

5. Voltage sag sources and extraction of their features

5.1. Short circuit as a source of voltage sag

Short circuits in the power system can be a source of voltage sag and cause some problems for customers. The amount of voltage drop depends on the type of fault, distance between the fault and point of study, system topology, and fault resistance. Moreover, the duration of the voltage sag depends on the protection systems. Faults are divided into 2 categories, symmetric and asymmetric; therefore, depending on the type of fault, the voltage drop in the 3 phases can be equal or unequal. In this study, symmetric faults are considered. The voltage sags generated by this type of fault are rectangular. The voltage drops suddenly and remains at a fixed value until the protection system operates. Figure 2 shows the waveform of the voltage sag caused by a symmetrical 3-phase short circuit and its IMFs, which are obtained by the EMD method.

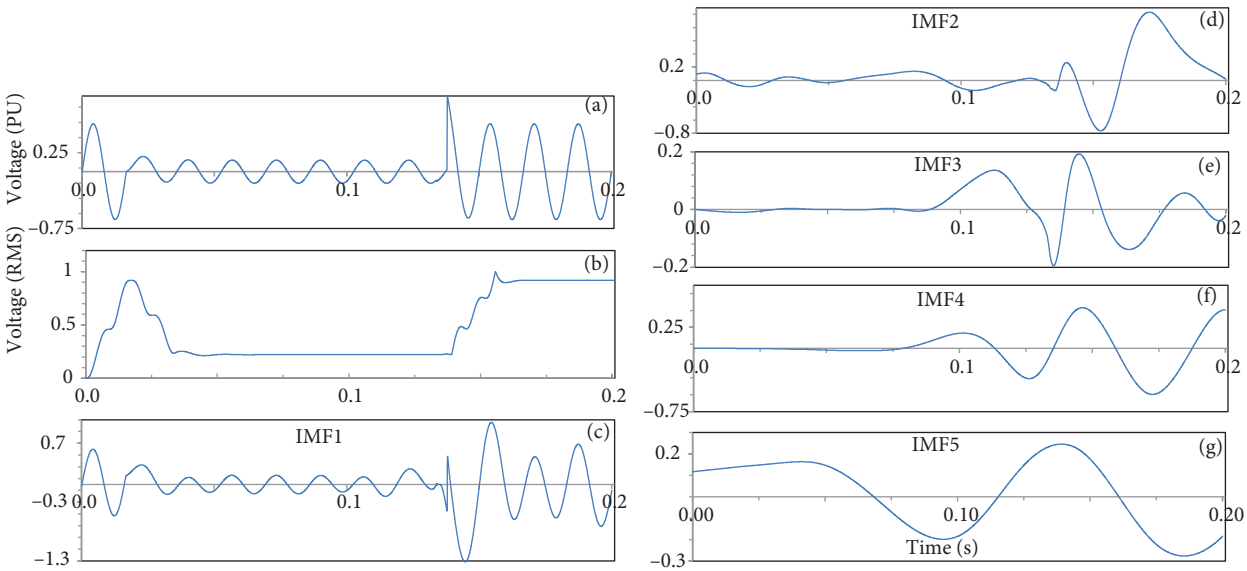

Figure 2. Voltage sag generated by the 3-phase short circuit (a and b) and IMFs (c–g).

Some general characteristics of a voltage sag waveform, which is generated by a symmetric short circuit, are as follows:

- Phase angle of the voltage varies due to this type of fault.
- There is no harmonic in the waveform.
- Voltage rapidly returns to the initial value.

The numerical model of this type of voltage is shown in Eq. (11):

$$V_A = [1 - s(u_1 - u_2)]\sin(2\pi f_1 t + \theta_A), \tag{11}$$

where s is the magnitude of voltage sag, u_1 and u_2 are the step functions, θ_A is the phase angle, f1 is the fundamental frequency, and t is the time. The range of t is $0 < t <$ duration with an interval of $1/f_s$, where f_s is the sampling frequency. The duration of the voltage sag can be determined by step functions (u_1 and u_2), as shown in Eq. (12), where the step functions can be determined by t_1, the starting time, and t_2, the ending time of the voltage sag.

$$u_n = \left\{ \begin{array}{l} 1 : \forall t \text{ if } t - t_n > 0 \\ 0 : \forall t \text{ if } t - t_n < 0 \end{array} \right\} \tag{12}$$

5.2. Transformer energizing as a source of voltage sag

Transformer energizing or a voltage variation in the transformer terminals can cause transformer saturation. Transformer saturation also generates voltage sag that is nonrectangular and contains harmonics. In Figure 3, a voltage sag waveform due to transformer energizing, the RMS waveform, and its IMFs are shown.

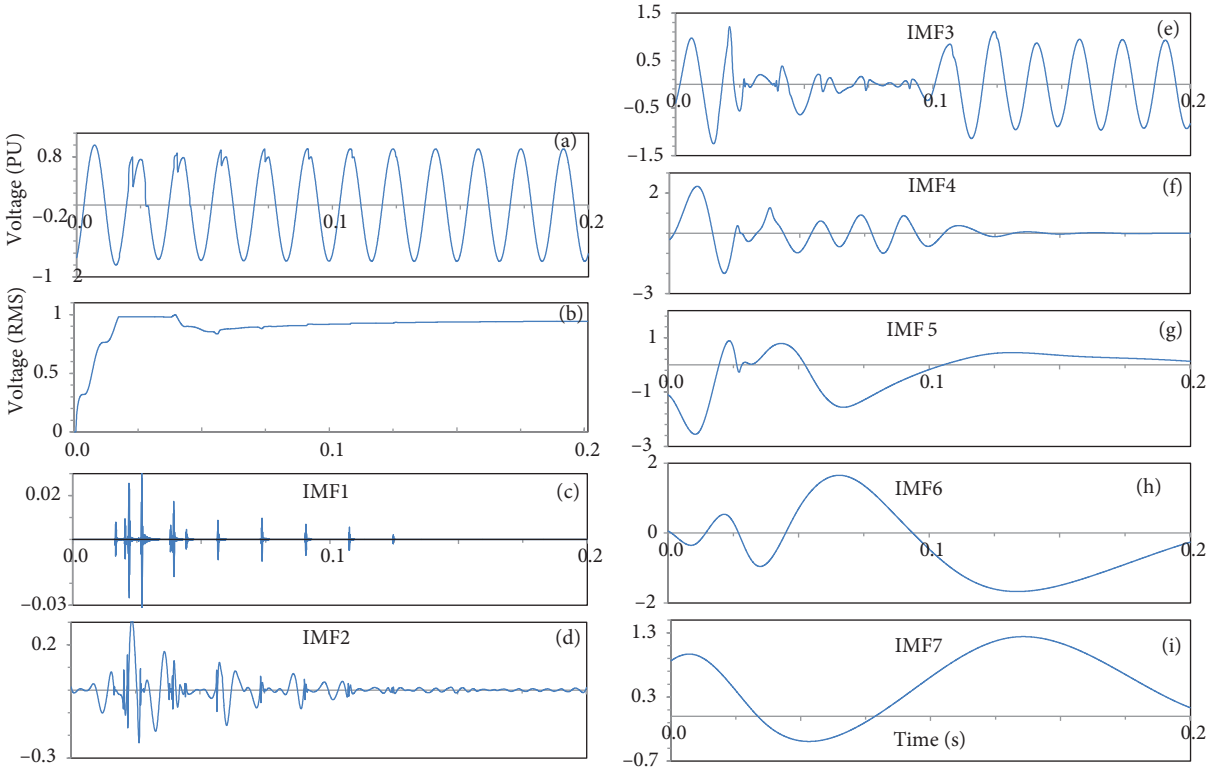

Figure 3. Voltage sag generated by transformer energizing (a and b) and IMFs (c–i).

The general characteristics of this voltage sag are:

- Asymmetrical voltage sag in the 3 phases.
- Low-voltage drop.

- No phase-angle variation.
- There are harmonics in the waveform.
- Voltage slowly returns to the initial value.

The numerical model of this type of voltage sag is stated in Eq. (13):

$$V_A = [1 - s(u_1.e^{-\alpha(t-t_1)})]\sin(2\pi f_1 t + \theta_A), \tag{13}$$

where t_1 is the starting time of the voltage sag, e is the exponential function for modeling the voltage sag due to transformer energizing, and α is the recovery rise rate.

5.3. Induction motor starting as a source of voltage sag

At the time of induction motor starting, the starting current is about 6 to 10 times that of the rated current. This high current causes voltage sag in the power system. The depth of this voltage sag and its duration depends on the size and features of the motor, strength of the power system at the point of motor connection, and methods of motor starting. Figure 4 illustrates a voltage sag waveform and its IMFs caused by induction motor starting. The maximum voltage drop due to motor starting is about 15% of the nominal voltage when the phase shift is about –6.6°. This phase shift compared with the phase shift due to a short circuit (maximum: –42.6) is very small.

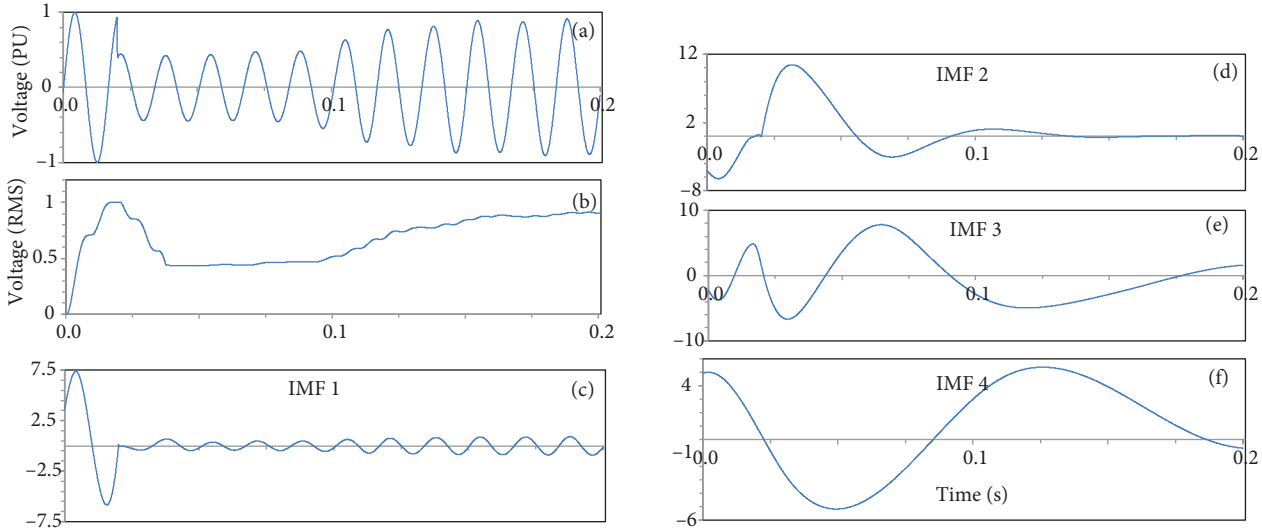

Figure 4. Voltage sag generated by induction motor starting (a and b) and IMFs (c–f).

The general features of this type of voltage sag are as follows:

- Symmetric voltage sag in the 3 phases.
- Low-depth voltage sag.
- Small phase shift.
- No harmonics.
- Voltage slowly returns to the initial value.

The numerical model of this type of voltage is shown in Eq. (14) where M_s is the voltage sag motor starting function, which is shown in Eq. (15), and M_r is the voltage sag recovery function, which can be obtained from Eq. (16). e is the exponential function used for modeling the motor starting voltage sag. β is the sag recovery rise rate, α is the sag decay rate, r is the ripple magnitude, f_r is the ripple frequency, and ρ is the ripple settling rate while the motor accelerates to its nominal speed.

$$V_A = [1 - s(M_s - M_r)]\sin(2\pi f_1 t + \theta_A) \tag{14}$$

$$M_s = u_1(1 - e^{-\alpha t_1}) + u_1(r\sin(2\pi f_r t_1)e^{-\rho t_1}) \tag{15}$$

$$M_r = u_2(1 - e^{-\beta t_1}) \tag{16}$$

5.4. Reacceleration of motors after fault clearance as a source of voltage sag

This type of voltage sag is generated in an area of the system in which motors are the major load of the system [18]. When a short circuit happens in the power system, the motor speed decreases. After fault clearance, the motor should act similar to the normal condition, so the motor should accelerate. This acceleration generates a voltage sag in the power system. When a fault occurs, the motor acts like a voltage source and prevents a sudden voltage drop [19]. After fault clearance, the voltage slowly returns to the initial value. In Figure 5, the waveform of this type of voltage sag and its IMFs are shown.

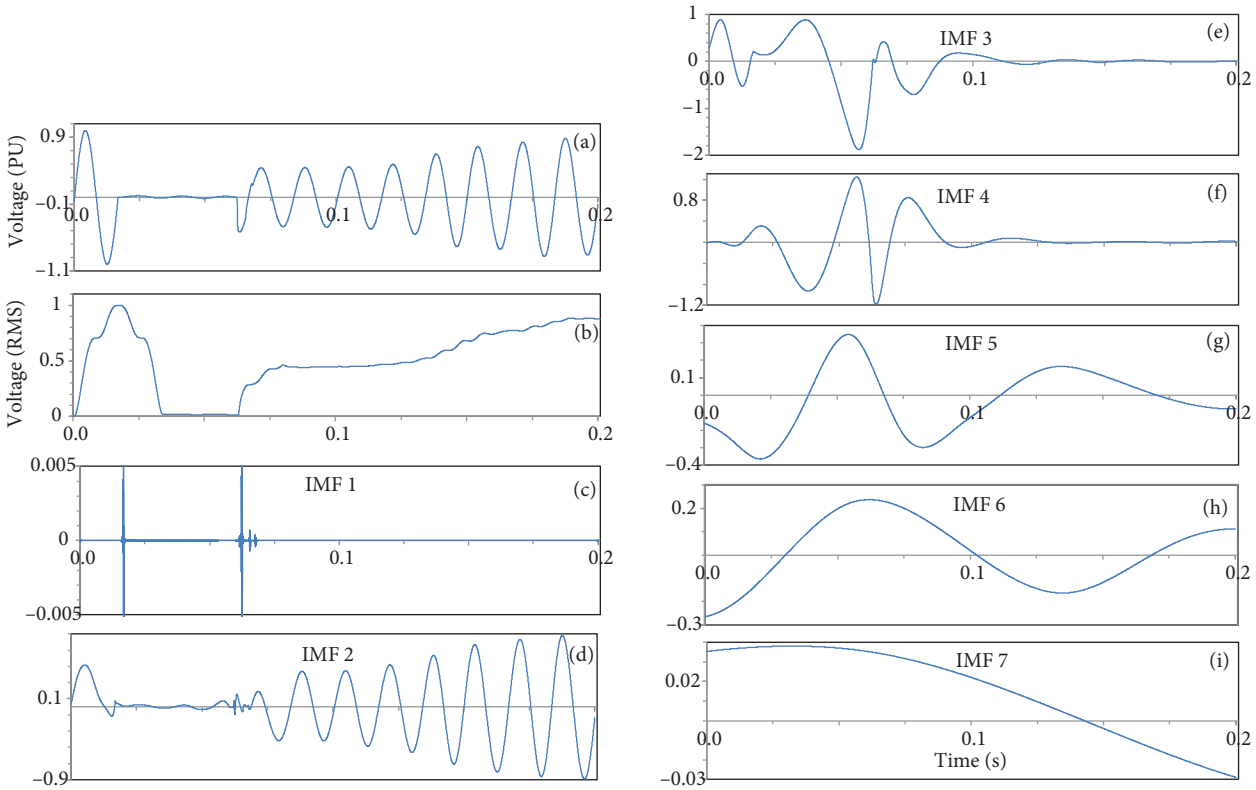

Figure 5. Voltage sag generated by reacceleration of large motors after fault clearance (a and b) and IMFs (c–i).

The general characteristics of this voltage sag are:

- Phase angle variation.
- No harmonics.
- Voltage slowly returns to the initial value.

The numerical model of this type of voltage sag is a combination of the numerical model of voltage sag due to short circuit and voltage sag due to motor starting.

6. Classification using SVM

Using artificial neural networks for classification has several disadvantages [20]. As the first disadvantage, the error function is multimodal, which includes many local minima. Thus, the learning process of this classifier can face problems. Moreover, they require a large number of data for training.

SVM is another classifier that is used widely because it does not have the above disadvantages. SVM uses a particular algorithm for maximizing the separating margin between 2 classes [21]. In the training process, a set of data pairs are given to the SVM.

$$(x_i, c_i), \text{ for } i = 1, 2, 3, \ldots, p \tag{17}$$

Here, x_i are the input vectors and c_i are the classes.

There are several activation functions that the SVM can use, such as sigmoid, linear, radial, and polynomial. The separating hyperplane g (x) for the linear separable training pairs of 2 classes is stated as in Eq. (18):

$$g(x) = w^T x + b = 0, \tag{18}$$

where w is the weight and b is the bias.

The hyperplane in Eq. (18) will be optimum when the separating margin between 2 classes is maximum. For achieving this purpose, Eq. (19) should be solved:

$$\min_w \frac{1}{2} w^T w, \tag{19}$$

subject to:

$$d_i(w^T x_i + b) \geq 1. \tag{20}$$

Eq. (19) is equal to minimizing the following Lagrange function:

$$J\{w, b, \alpha\} = \frac{1}{2}(w^T w) - \sum\nolimits_{i=1}^{p} \alpha_i [d_i(w^T x_i + b) - 1]. \tag{21}$$

In Eq. (21), α_i is a nonzero Lagrange coefficient.

The above objective function is valid if 2 classes are distributed linearly. Thus, if the distribution of 2 classes is nonlinear, a new objective function, as in Eq. (22), should be implemented.

$$\min \frac{1}{2} w^T w + C \sum_{i=1}^{p} \xi_i, \xi_i) 0 \tag{22}$$

$$\text{Subject to } d_i(w^T\phi(x_i)+b) \geq 1-\xi_i \tag{23}$$

In the above equations, ξ is the fulfilling variable and C is the upper bound of α.

Vector x_i is mapped into a higher dimensional space by function ϕ. The kernel function is defined as: $K(x_i,x_j) = \phi(x_i)^T\phi(x_j)$. Different kernel functions can be used. Some of the kernel functions used in this paper are presented as follows:

1. Linear kernel:

$$K(x_i,x_j) = x_i^T x_j. \tag{24}$$

1. Polynomial kernel:

$$K(x_i,x_j) = (\gamma x_i^T x_j + r)^d, \gamma > 0. \tag{25}$$

1. Gaussian radial basis function (RBF) kernel:

$$K(x_i x_j) = exp(-\gamma||x_i - x_j||^2), \gamma > 0. \tag{26}$$

In the above functions, r, d, and γ are kernel parameters.

SVM finds the best separating margin between 2 classes by optimizing the above equations.

7. Results and discussion

In this paper, for the detection and classification of voltage sources in the power system, the EMD method is used for obtaining the first 3 IMFs. Next, by applying the Hilbert transform on these 3 IMFs, the features of each IMF, including the standard deviation of the amplitude, standard deviation of the phase, and energy distribution, are obtained. In the next step, these features are given to the SVM for detection and classification according to the source of the voltage sag. Figure 6 shows a diagram of the voltage sag classification using the HHT and SVM. In this study, as shown in the previous section, 4 voltage sag sources are considered. These sources include voltage sag caused by short circuit (S_1), voltage sag caused by transformer energizing (S_2), voltage sag caused by motor starting (S_3), and voltage sag caused by reacceleration of large motors after fault clearance (S_4).

Some of the information and parameters used in the simulation are as follows:

Fault: A symmetrical fault is considered. The starting and the ending time of the voltage sags are 0.016 s and 0.18 s, respectively. A 3-phase short circuit is applied to the power system network with different values for the fault resistance. The simulation results of this study show that the phase shift due to the short circuit varies between –13.8° and –42.6°.

Transformer: For generating this type of voltage sag, a 500-kV power system network, including a 500/375-kV double-winding transformer, is energized for simulating.

Motor: For this case, a 400-V power system network is chosen. The motor types and typical electrical parameters of the induction motors used in this study for generating the voltage sag are presented in Table 2. In addition, the schematic of the simulated system, to generate voltage sag due to motor starting, can be seen in Figure 7. The maximum voltage drop due to motor starting is about 85% of the nominal voltage, where the phase shift is about –6.6°.

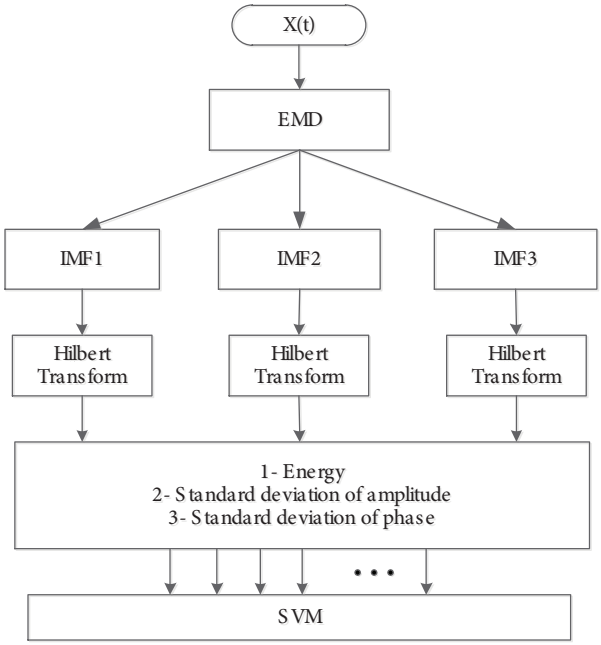

Figure 6. Diagram of the proposed classification method.

Table 2. Motor types and typical electrical parameters.

Motor types							
5.4 HP, 4 kW, 400 V, 50 Hz, 1430 RPM	10 HP, 7.5 kW, 400 V, 50 Hz, 1440 RPM	20 HP, 15 kW, 400 V, 50 Hz, 1460 RPM	50 HP, 37 kW, 400 V, 50 Hz, 1480 RPM	100 HP, 75 kW, 400 V, 50 Hz, 1484 RPM	150 HP, 10 kW, 400 V, 50 Hz, 1487 RPM		
Typical electrical parameters							
Stator resistance (ohm)	Stator inductance (H)	Rotor resistance (ohm)	Rotor inductance (H)	Mutual inductance (H)	Inertia	Friction factor (N m s)	Pole pairs
1.115	0.005974	1.083	0.005974	0.2037	0.02	0.005752	2

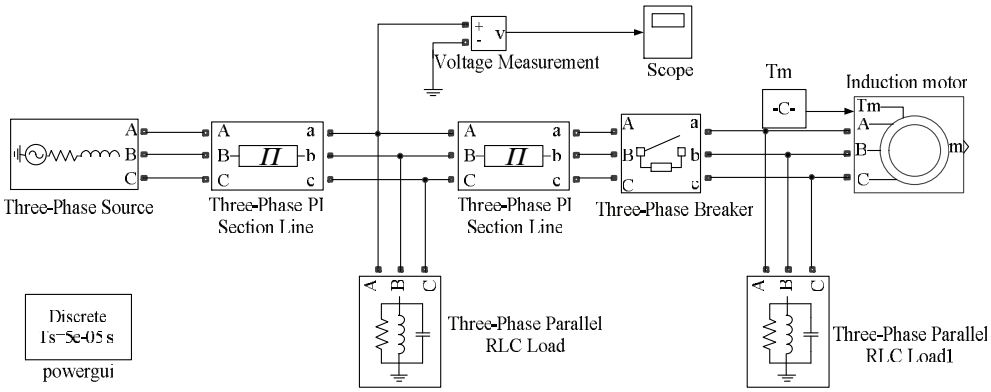

Figure 7. Schematic of simulated system for generating voltage sag due to motor starting.

All of the voltage sag waveforms from the 4 voltage sag sources are generated using MATLAB/Simulink and mathematical models of the voltage sags are stated in Section 5. Using MATLAB/Simulink and the

mathematical model of the voltage sag sources together helps to generate different types of voltage sags with a wide range of variation in the depth, duration, etc. For each type, 145 sag waveforms are generated, from which 45 sag waveforms are selected for training of the SVM and 100 sag waveforms are used for testing of the SVM. Table 3 shows the results of the proposed classification method. For demonstrating the superiority of the proposed method, the results of the proposed method are compared with the results of the classification method using the wavelet transform with a probabilistic neural network (PNN) [10] and the results of classification using a PNN and EMD. This comparison is given in Table 4. A comparison of the results of the proposed method, which uses EMD and SVM, with the results of 2 other methods shows the high efficiency and better accuracy of the proposed method. For obtaining this efficiency, different kernel functions, including linear, polynomial, and Gaussian RBF, are used. These functions are presented in Section 6. The best efficiency (99.5%) is obtained using the polynomial kernel function with these parameters: C = 100, d = 5.

Table 3. EMD and SVM classification method results.

EMD and SVM method	S1	S2	S3	S4	Classification efficiency (%)	Overall efficiency (%)
S1	100	0	0	0	100	99.5
S2	0	99	1	0	99	
S3	0	0	100	0	100	
S4	1	0	0	99	99	

Table 4. Comparison of the results of the proposed method with EMD and a PNN, and a wavelet and a PNN.

EMD and SVM method	S1	S2	S3	S4	Classification efficiency (%)	Overall efficiency (%)
S1	100	0	0	0	100	99.5
S2	0	99	1	0	99	
S3	0	0	100	0	100	
S4	1	0	0	99	99	
Wavelet and PNN method	S1	S2	S3	S4		
S1	50	0	0	NC	100	84.37
S2	0	38	12	NC	76	
S3	11	0	39	NC	78	
EMD and PNN method	S1	S2	S3	S4		
S1	98	0	0	2	98	96.75
S2	0	92	8	0	92	
S3	0	0	100	0	100	
S4	1	0	2	97	97	

NC: Not considered.

The efficiencies of using different kernel functions are presented in Table 5.

Table 5. Comparison of the results of using SVM with different kernel functions.

	Correct rate of recognition (%)				
Different kernel functions	Fault	Motor starting	Transformer energizing	Motor reacceleration	Overall efficiency (%)
Linear kernel	95	92	74	91	88
RBF kernel	98	97	96	99	97.5
Polynomial kernel	100	100	99	99	99.5

In this study, another voltage sag source (S_4), voltage sag due to reacceleration of large motors after faults clearance, is considered, which was not considered in [10]. It is obvious from the results that the SVM is stronger than the PNN for classifying voltage sag sources.

8. Conclusions

In this paper, a new method for the detection and classification of voltage sag sources was proposed. Four source of voltage sag were considered, including a 3-phase short circuit, motor starting, transformer energizing, and reacceleration of large motors after fault clearance. In the proposed method, the HHT and SVM were used for classification. After obtaining the first 3 IMFs of each voltage sag waveform, 3 features from each IMF, including the standard deviation of the amplitude, standard deviation of the phase, and energy distribution, were extracted and these features were given to the SVM for classification. The results of the proposed classification method were compared with 2 other methods: the wavelet transform with a PNN and EMD with a PNN. In addition, for obtaining the highest efficiency, different kernel functions were used in the SVM. The obtained results from the proposed method demonstrated the high efficiency, accuracy, and the superiority of the proposed method for the classification of voltage sag sources.

References

[1] S. Santoso, H.W. Beaty, R.C. Dugan, M.F. McGranaghan, Electrical Power Systems Quality, New York, McGraw-Hill Professional, 2002.

[2] W.M. Lin, C.H. Wu, C.H. Lin, F.S. Cheng, "Detection and classification of multiple power-quality disturbances with wavelet multiclass SVM", IEEE Transactions on Power Delivery, Vol. 23, pp. 2575–2582, 2008.

[3] S. Mishra, C.N. Bhende, B.K. Panigrahi, "Detection and classification of power quality disturbances using S-transform and probabilistic neural network", IEEE Transactions on Power Delivery, Vol. 23, pp. 280–287, 2008.

[4] S. Shukla, S. Mishra, B. Singh, "Empirical-mode decomposition with Hilbert transform for power-quality assessment", IEEE Transactions on Power Delivery, Vol. 24, pp. 2159–2165, 2009.

[5] S. Djokic, J.V. Milanovic, D.J. Chapman, M.F. McGranaghan, "Shortfalls of existing methods for classification and presentation of voltage reduction events", IEEE Transactions on Power Delivery, Vol. 20, pp. 1640–1649, 2005.

[6] M. Manjula, A.V.R.S. Sarma, S. Mishra, "Detection and classification of voltage sag causes based on empirical mode decomposition", Annual IEEE India Conference, pp. 1–5, 2011.

[7] F. Xu, Y. Zhang, H. Yang, X. Xiao, "Classification for voltage sags based on generalized S-transform", 9th International Conference on Fuzzy Systems and Knowledge Discovery, pp. 1760–1763, 2012.

[8] N. Ding, W. Cai, J. Suo, J. Wang, Y. Xu, "Voltage sag disturbance detection based on RMS voltage method", Power and Energy Engineering Conference, pp. 1–4, 2009.

[9] C.I. Chen, H.L. Wang, Y.C. Chin, "A simple rule-based approach for detection and classification of voltage sag, swell, and interruption in power systems", IEEE Ninth International Conference on Power Electronics and Drive Systems, pp. 756-762, 2011.

[10] M. Manjula, A.V.R.S. Sarma, G.V. Naga Lakshmi, "Wavelet transform for classification of voltage sag causes using probabilistic neural network", International Journal of Electrical Engineering, Vol. 4, pp. 299–309, 2011.

[11] S. Kamble, C. Thorat, "Classification of voltage sags in distribution systems due to short circuit faults", 13th International Conference on Optimization of Electrical and Electronic Equipment, pp. 257–264, 2012.

[12] N.E. Huang, M.L.C. Wu, S.R. Long, S.S.P. Shen, W. Qu, P. Gloersen, K.L. Fan, "A confidence limit for the empirical mode decomposition and Hilbert spectral analysis", Proceedings of the Royal Society A, Vol. 459, pp. 2317–2345, 2003.

[13] E. Huang, Z. Shen, and S.R. Long, "The empirical mode decomposition and the Hilbert spectrum for nonlinear and non-stationary time series analysis", Proceedings of The Royal Society A, Vol. 454, pp. 903–995, 1998.

[14] B. Barnhart, The Hilbert-Huang transform: theory, applications, development, PhD, University of Iowa, Iowa City, IA, USA, 2011.

[15] R.N. Bracewell, The Fourier Transform and Its Applications, New York, McGraw Hill, 2000.

[16] S.G. Mallat, "A theory for multiresolution signal decomposition: the wavelet representation", IEEE Transactions on Pattern Analysis and Machine Intelligence, Vol. 11, pp. 674–693, 1989.

[17] J.S. Bendat, The Hilbert Transform and Applications to Correlation Measurements, Naerum, Denmark, Brüel & Kjaer, 1985.

[18] M.H.J. Bollen, "The influence of motor reacceleration on voltage sags", IEEE Transactions on Industry Applications, Vol. 31, pp. 667–674, 1995.

[19] M. Kezunovic, Y. Liao, "A new method for classification and characterization of voltage sags", Electric Power Systems Research, Vol. 58, pp. 27–35, 2001.

[20] D.W. Patterson, Artificial Neural Networks: Theory and Applications, Singapore, Prentice Hall, 1996.

[21] C. Burges, "A tutorial on support vector machines for pattern recognition", Data Mining and Knowledge, Vol. 2, pp. 121–167, 1998.